Volume 14
Number 15
21 April 2023
Pages 3951–4194

Chemical Science

rsc.li/chemical-science

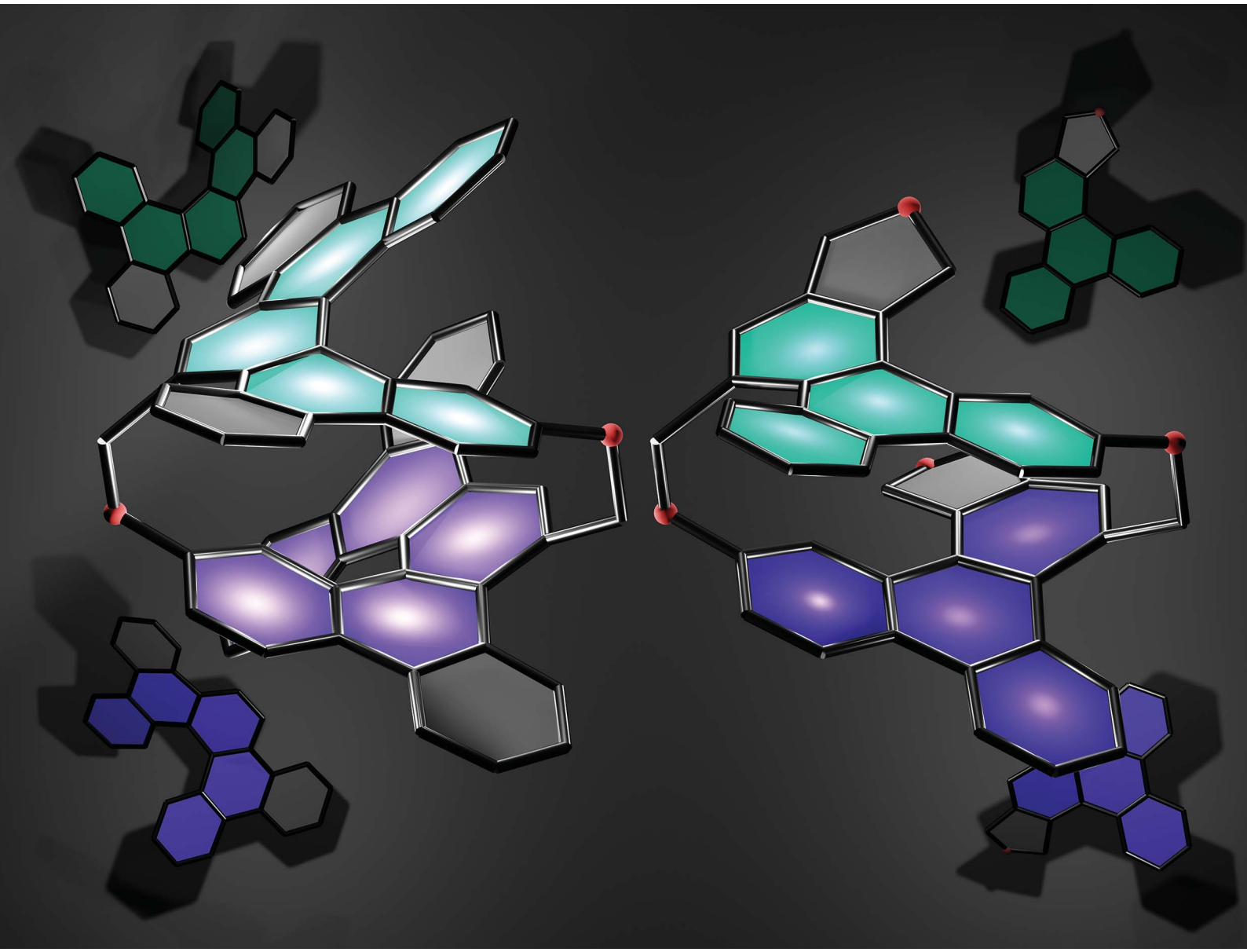

ISSN 2041-6539

ROYAL SOCIETY OF CHEMISTRY

EDGE ARTICLE

Yuya Kawai *et al.*

Stereoselective synthesis of [2.2]triphenylenophanes *via* intramolecular double [2 + 2 + 2] cycloadditions

Chemical Science

ROYAL SOCIETY OF CHEMISTRY

EDGE ARTICLE

View Article Online
View Journal | View Issue

Check for updates

Cite this: *Chem. Sci.*, 2023, **14**, 3963

All publication charges for this article have been paid for by the Royal Society of Chemistry

Received 2nd February 2023
Accepted 9th March 2023

DOI: 10.1039/d3sc00571b

rsc.li/chemical-science

Open Access Article. Published on 10 March 2023. Downloaded on 2/5/2026 11:14:31 AM.
This article is licensed under a Creative Commons Attribution 3.0 Unported Licence.

Stereoselective synthesis of [2.2] triphenylenophanes *via* intramolecular double [2 + 2 + 2] cycloadditions†

Yuya Kawai, Juntaro Nogami, Yuki Nagashima and Ken Tanaka *

Planar chiral [2.2]cyclophanes with two aromatic rings in close proximity have attracted much attention for their applications as chiral materials and catalysts because of their stable chirality and transannular interactions. Although numerous [2.2]cyclophanes have been synthesized to date, only a few polycyclic aromatic hydrocarbon (PAH)-based ones have been reported, and the simultaneous control of two planar chiralities of the two aromatic rings facing each other has not been achieved. Here we report the enantio- and/or diastereoselective synthesis of planar chiral PAH-based [2.2]cyclophanes ([2.2] triphenylenophanes) *via* the high-yielding base-mediated intermolecular macrocyclization and Rh- or Ni-catalyzed intramolecular double [2 + 2 + 2] cycloadditions. DFT calculations have revealed that the second [2 + 2 + 2] cycloaddition kinetically determines the diastereoselectivity. Single crystal X-ray diffraction analyses have confirmed that the facing triphenylene or [5]helicene skeletons strongly repel each other, resulting in curved structures with bulged centers.

Introduction

Cyclophanes are macrocyclic compounds with a structure in which an aromatic unit is linked into a ring by an ansa chain.[1] In particular, cyclophanes with two stacked aromatic rings, such as [*n*.*n*]paracyclophanes, have long attracted attention due to their unique properties.[2] In [2.2]paracyclophanes, where the tether length is two atoms, the interplanar distance is shorter than the interlayer distance of graphene.[3] This short distance results in an electronic transannular interaction between the two aromatic rings,[4] highly curved aromatic rings due to steric repulsion,[5] and stable planar chirality due to rotational inhibition.[6] Planar chiral polycyclic aromatic hydrocarbon (PAH)-based [2.2]cyclophanes are highly attractive because of their chiral nanographite-like structure.[7] However, the linkage of two large PAHs with two-atom tethers is troublesome due to difficulty in controlling steric hindrance and stereoselectivity. Thus stepwise π-elongation syntheses from planar chiral [2.2]paracyclophane derivatives have been reported, although their structures are restricted to molecules with a [2.2]paracyclophane core (Fig. 1a, top).[8,9] Morisaki and co-workers reported the synthesis of [2.2][4]helicenophane by oxidative photocyclization of a planar chiral stilbene-type precursor.[8] As an exceptional example of the stereoselective direct linkage of two large PAHs with two-atom tethers, Bodwell and co-workers reported the isolation of planar chiral [2.2]pyrenophane as an unexpected side product from the intramolecular McMurry coupling of [10.2]pyrenophane-dialdehyde, presumably through the intramolecular McMurry coupling of the corresponding linear dialdehyde (Fig. 1a, bottom).[10,11] However, this shadow reaction was not confirmed experimentally. In addition, inserting an atom with a van der Waals radius shorter than the carbon atom into the tether of the [2.2]paracyclophane is troublesome, and no synthetic examples have been reported to date.[12]

Furthermore, the asymmetric synthesis of stacked [*n*.*n*] cyclophanes is more troublesome than that of [*n*]cyclophanes. Our group[13a] and the Shibata group[13b] reported only two examples each of introducing planar chirality on only one side (Fig. 1b). These syntheses have moderate enantioselectivity and structural limitations that prevent shortening the tether length. Thus [*n*.*n*]cyclophanes with planar chirality on both sides have been supplied by the optical resolution of racemates. As a representative example, Morisaki and co-workers reported the optical resolution of planar chiral tetrasubstituted [2.2]paracyclophane derivatives for synthesizing a propeller-shaped macrocyclic compound, showing high fluorescence quantum efficiency and an excellent circularly polarized luminescence dissymmetry factor (Fig. 1c).[14,15]

On the other hand, Rh-catalyzed [2 + 2 + 2] cycloadditions[16–18] allow enantioselective control of the planar chirality of [*n*] cyclophanes.[19] Here, we report the stereoselective synthesis of oxamethylene-bridged PAHs-based [2.2]cyclophanes ([2.2]triphenylenophanes) **3** *via* the base-mediated intermolecular

Department of Chemical Science and Engineering, Tokyo Institute of Technology, O-okayama, Meguro-ku, Tokyo 152-8550, Japan. E-mail: ktanaka@apc.titech.ac.jp

† Electronic supplementary information (ESI) available. CCDC 2237885 and 2237886. For ESI and crystallographic data in CIF or other electronic format see DOI: https://doi.org/10.1039/d3sc00571b

© 2023 The Author(s). Published by the Royal Society of Chemistry

Open Access Article. Published on 10 March 2023. Downloaded on 2/5/2026 11:14:31 AM.
This article is licensed under a Creative Commons Attribution 3.0 Unported Licence.

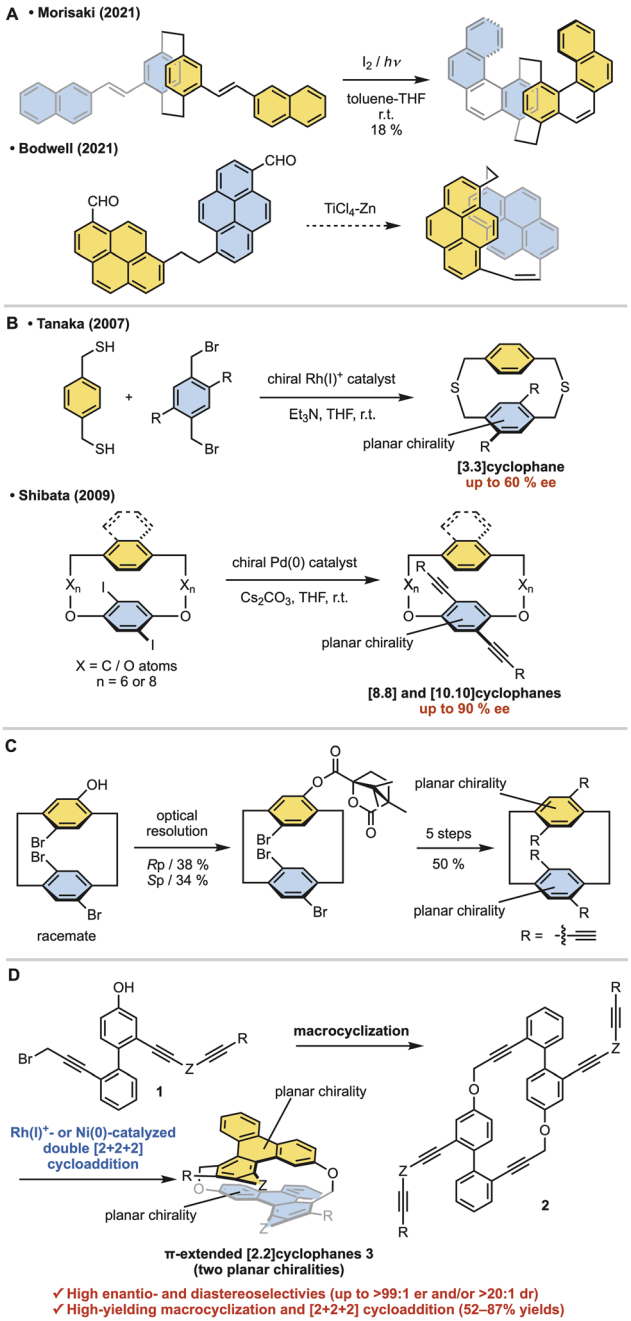

Fig. 1 Research backgrounds. (A) Synthesis of racemic planar chiral π-extended [2.2]cyclophanes. (B) Enantioselective synthesis of [*n.n*] cyclophanes with one planar chirality. (C) Optical resolution of racemic [2.2]cyclophane with two planar chiralities (Morisaki, 2014). (D) Enantio- and diastereoselective synthesis of π-extended [2.2]cyclophanes (this work).

macrocyclization of triynes **1**, leading to cyclic hexaynes **2**, and the subsequent Rh- or Ni-catalyzed intramolecular double [2 + 2 + 2] cycloadditions[20–22] (Fig. 1d). The present stereoselective synthesis realizes high enantioselectivity (up to >99 : 1 er) and complete diastereoselectivity (>20 : 1 dr). Furthermore, the yields of two key reaction steps (the macrocyclization and double [2 + 2 + 2] cycloadditions) are high. Notably, the present asymmetric [2.2]cyclophane synthesis is the first example of diastereo- and enantioselective control of two planar chiralities of the [*n.n*]cyclophanes.

Results and discussion

First, we examined the synthesis of cyclic hexaynes for the asymmetric intramolecular double [2 + 2 + 2] cycloadditions, as shown in Fig. 2. MOM-protection of 4-bromo-3-iodophenol (**4**) gave bromide **5**, and the subsequent Sonogashira cross-coupling with diynes **6a–e** gave diynes **7a–e** in high yields (78–86%). The Suzuki–Miyaura cross-coupling between bromides **7a–e** and boronic acid **8** followed by deprotection of the silyl protecting group by treatment with TBAF gave alcohols **9a–e** in moderate yields. Treatment of **9a–e** with Br_2 and PPh_3 afforded bromo-phenols **1a–e**, in which the bromination of the propargylic alcohol and the deprotection of the MOM protecting group proceeded in one pot. Pleasingly, the base (K_2CO_3)-mediated intermolecular macrocyclization gave cyclic hexaynes **2a–e** in good yields. Although the base-mediated intermolecular macrocyclization generally yields a mixture of dimers, trimers, and other oligomers,[20] the ^1H NMR analyses of the crude reaction mixtures derived from **1a–e** confirmed the selective formations of the dimers (hexaynes) **2a–e** in this process (Fig. S1†).

Next, we investigated the asymmetric synthesis of [2.2]triphenylenophanes (Table 1). In the presence of 80 mol% of the cationic rhodium(I)/BIPHEP complex, intramolecular double [2 + 2 + 2] cycloadditions of cyclic hexayne **2a** proceeded at room temperature to give the desired [2.2]triphenylenophane **3a** in a high 87% yield (entry 1, 93% yield per each [2 + 2 + 2] cycloaddition).[23] Interestingly, the reaction proceeded in complete diastereoselectivity [dr(dl/*meso*) = >20 : 1]. We subsequently

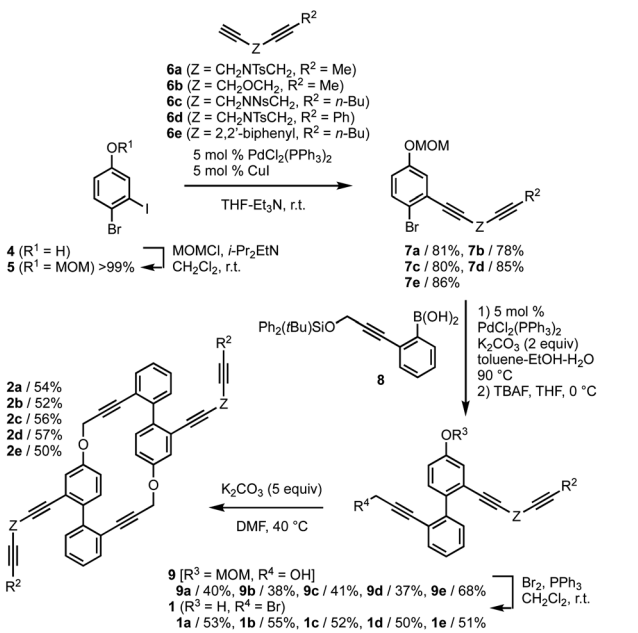

Fig. 2 Synthesis of hexaynes **2**. MOM = methoxylmethyl. Ts = *p*-toluenesulfonyl. Ns = 2-nitrobenzenesulfonyl. TBAF = tetrabutylammonium fluoride.

© 2023 The Author(s). Published by the Royal Society of Chemistry

Open Access Article. Published on 10 March 2023. Downloaded on 2/5/2026 11:14:31 AM.
This article is licensed under a Creative Commons Attribution 3.0 Unported Licence.

Table 1 Double [2 + 2 + 2] cycloadditions of hexaynes **2** leading to [2.2]triphenylenophanes **3**

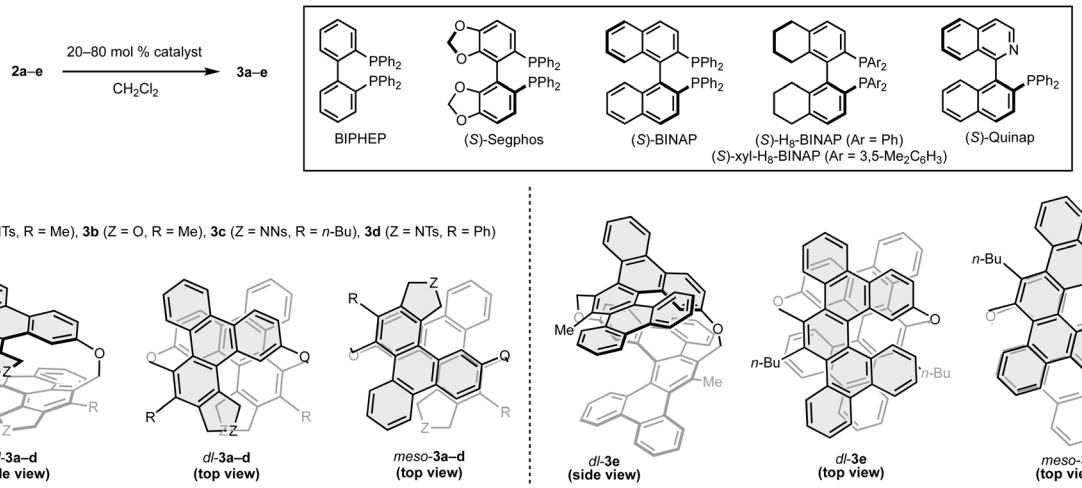

Entry	2	Catalyst	Catalyst (mol%)	Temp, time	3/% yield[a] (dl/*meso*, er)
1	**2a**	$[Rh(cod)_2]BF_4$/BIPHEP	80	r.t, 3 h	**3a**/87 (>20 : 1)
2	**2a**	$[Rh(cod)_2]BF_4$/(*S*)-segphos	80	r.t, 3 h	(+)-**3a**/82 (>20 : 1, 84 : 16)
3	**2a**	$[Rh(cod)_2]BF_4$/(*S*)-BINAP	80	r.t, 3 h	(+)-**3a**/84 (>20 : 1, 88 : 12)
4	**2a**	$[Rh(cod)_2]BF_4$/(*S*)-H_8-BINAP	80	r.t, 3 h	(+)-**3a**/80 (>20 : 1, 93 : 7)
5	**2a**	$[Rh(cod)_2]BF_4$/(*S*)-xyl-H_8-BINAP	80	r.t, 3 h	(+)-**3a**/21 (>20 : 1, >99 : 1)
6	**2a**	$[Rh(cod)_2]BF_4$/(*S*)-H_8-BINAP	20	r.t, 3 h	(+)-**3a**/84 (>20 : 1, 95 : 5)
7	**2b**	$[Rh(cod)_2]BF_4$/(*S*)-H_8-BINAP	20	r.t, 3 h	(*R*p,*R*p)-(+)-**3b**/82 (>20 : 1, 93 : 7)
8	**2c**	$[Rh(cod)_2]BF_4$/(*S*)-H_8-BINAP	20	r.t, 3 h	(+)-**3c**/82 (>20 : 1, 94 : 6)
9	**2d**	$[Rh(cod)_2]BF_4$/(*S*)-H_8-BINAP	20	r.t, 3 h	**3d**/insoluble
10	**2e**	$[Rh(cod)_2]BF_4$/(*S*)-H_8-BINAP	20	r.t, 3 h	No reaction
11[b]	**2e**	$[Rh(cod)_2]BF_4$/(*S*)-H_8-BINAP	20	60 °C, 16 h	Complex mixture
12	**2e**	$Ni(cod)_2$/2PPh_3	20	40 °C, 16 h	**3e**/83 (>20 : 1)
13	**2e**	$Ni(cod)_2$/(*S*)-Quinap	20	40 °C, 16 h	Complex mixture

[a] Isolated yield. [b] $(CH_2Cl)_2$ was used instead of CH_2Cl_2.

examined the enantioselective synthesis of **3a** by using axially chiral biaryl bisphosphine ligands and found that enantioselectivity increases with increasing bite angle (entries 2–4, bite angle:[24] Segphos < BINAP < H_8-BINAP). Although the use of sterically demanding xyl-H_8-BINAP afforded **3a** in the highest enantioselectivity (>99 : 1 er), the product yield was the lowest 21% due to the undesired intermolecular [2 + 2 + 2] cycloaddition (entry 5). Reducing the catalyst loading to 20 mol% maintained the high yield and enantioselectivity (entry 6). Thus, the conditions of entry 6 were set as the optimum conditions.

The yields, enantioselectivity, and diastereoselectivity of the products **3b** and **3c** were all favorable when the linker moiety of the 1,6-diyne side chain was changed from NTs to O and NNs (**2b** and **2c**, entries 7 and 8). However, in the reaction of hexayne **2d** with a phenyl group at the terminus of the 1,6-diyne side chain, **2d** disappeared completely, but a solid with extremely low solubility was formed (entry 9). We also investigated the synthesis of [2.2][5]helicenophane **3e**, which is further π-extended from [2.2]triphenylenophanes, by replacing the 1,6-diyne side chain with a biphenyl-linked 1,7-diyne one (**2e**). Although we carried out the reaction of hexayne **2e** under the above optimal conditions, no conversion of **2e** was observed (entry 10). At an elevated reaction temperature of 60 °C, a complete conversion of **2e** was observed, but the desired product **3e** was not generated at all (entry 11). Pleasingly, the desired intramolecular double [2 + 2 + 2] cycloadditions of **2e** proceeded at 40 °C in a high 83% yield and complete diastereoselectivity by using the nickel(0)/PPh_3 complex (entry 12).[25] Stáry and co-workers reported that Quinap is a highly effective chiral ligand for the enantioselective synthesis of carbohelicenes by the nickel(0)-catalyzed intramolecular [2 + 2 + 2] cycloaddition.[26] Thus, we also investigated the enantioselective synthesis of **3e** using Quinap as a chiral ligand, but a complex mixture of products was generated (entry 13).

The above intramolecular double [2 + 2 + 2] cycloaddition reactions yield cyclophanes **3** with high enantioselectivity and complete diastereoselectivity. Thus, we analyzed the steps in which stereoselectivities are determined using cyclic hexayne **2b** and (*S*)-H_8-BINAP as a substrate and ligand, respectively (Fig. 3). The first [2 + 2 + 2] cycloaddition of **2b** produces four possible intermediates (*R*p,*S*a)-**IM0**, (*R*p,*R*a)-**IM0**, (*S*p,*R*a)-**IM0**, and (*S*p,*S*a)-**IM0** with one planar chiral triphenylene moiety and one axially chiral biphenyl moiety (Fig. 3a). The triphenylene moieties of **IM0** are sufficiently large relative to the tether length that those are non-rotatable at room temperature,[19c–f] and thus the first [2 + 2 + 2] cycloaddition would enantioselectively

Open Access Article. Published on 10 March 2023. Downloaded on 2/5/2026 11:14:31 AM.
This article is licensed under a Creative Commons Attribution 3.0 Unported Licence.

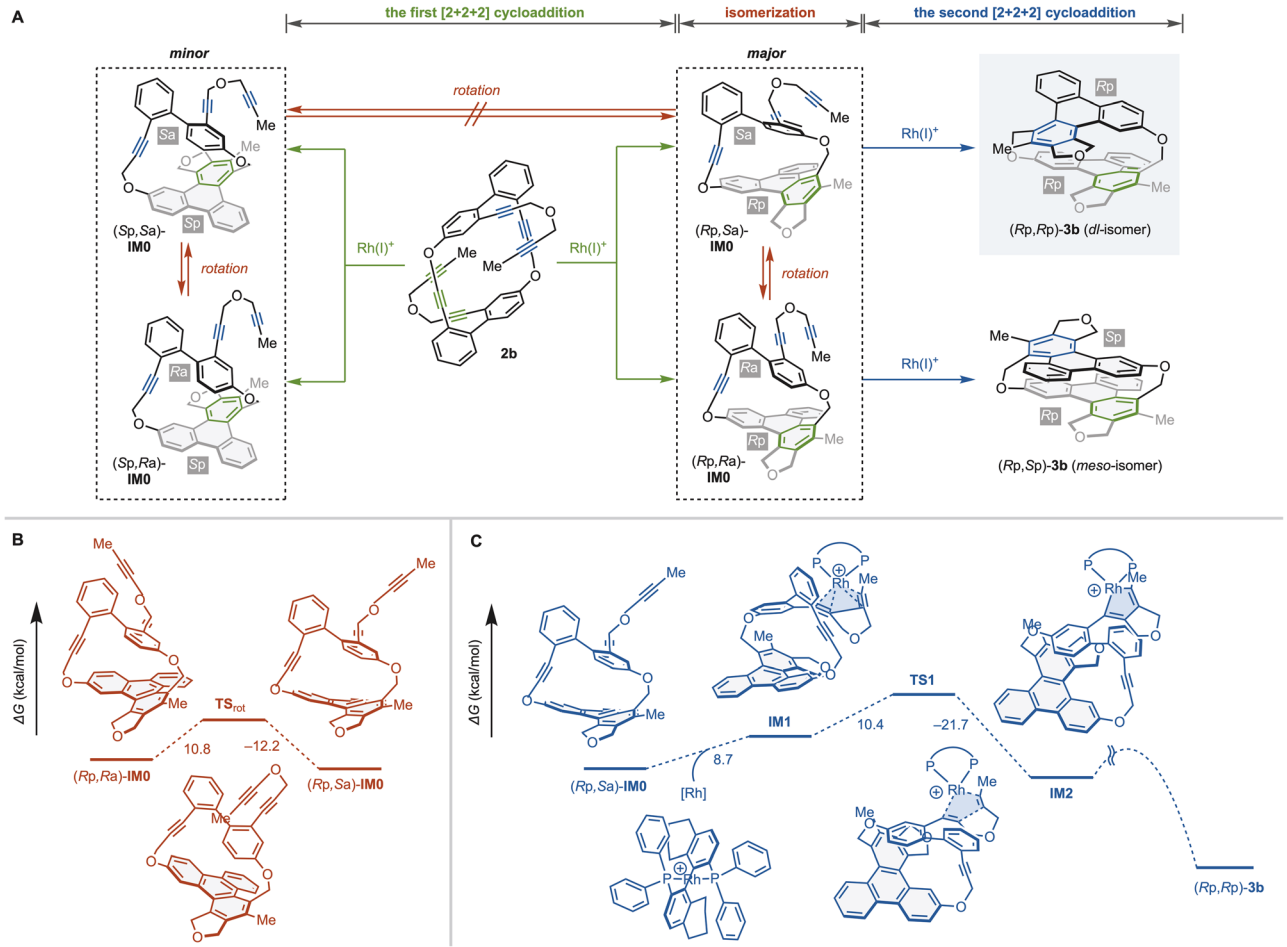

Fig. 3 Analyses for steps determining enantio- and diastereoselectivities to produce (*Rp*,*Rp*)-**3b** from **2b**. The changes of the Gibbs free energies (kcal mol^{-1}) are calculated at the M06/6-31G(d) (C, H, O, P) and LANL2DZ (Rh) level. (A) Reaction pathways of Rh-catalyzed [2 + 2 + 2] cycloaddition of **2b** leading to **3b**. (B) Rotation isomerization of axial chirality. (C) The second [2 + 2 + 2] cycloaddition to produce (*Rp*,*Rp*)-**3b**.

determine the planar chirality, producing (*Rp*,*Sa*)-**IM0** and (*Rp*,*Ra*)-**IM0**.

The step determining the diastereoselectivity may be the rotational isomerization of the axial chirality or the first or second [2 + 2 + 2] cycloaddition (Fig. 3a). We performed DFT calculations at the M06/6-31G(d)&LANL2DZ level to elucidate which step determines the diastereoselectivity. DFT calculations estimate the activation energies of the biphenyl rotation to be $\Delta G^{\ddagger}_{\mathrm{TSrot\text{-}(Rp,Ra)\text{-}IM0}} = 10.8$ kcal mol^{-1} and $\Delta G^{\ddagger}_{\mathrm{TSrot\text{-}(Rp,Sa)\text{-}IM0}} = 12.2$ kcal mol^{-1}, indicating that the rotational isomerization proceeds rapidly even at room temperature (Fig. 3b). We then explored the reaction pathway of the second [2 + 2 + 2] cycloaddition of (*Rp*,*Sa*)-**IM0** leading to (*Rp*,*Rp*)-**3b** (Fig. 3c).[27,28] We found that the activation energy for the rate-limiting five-membered rodacycle formation [(*Rp*,*Sa*)-**IM0** → **IM1** → **TS1**, $\Delta G^{\ddagger} = 19.1$ kcal mol^{-1}] is more than 6 kcal mol^{-1} larger than the rotational isomerization between (*Rp*,*Sa*)-**IM0** and (*Rp*,*Ra*)-**IM0**. Thus we can conclude that the second [2 + 2 + 2] cycloaddition kinetically determines the diastereoselectivity.

We performed single-crystal X-ray diffraction analyses of [2.2]triphenylenophane (±)-**3a** (Fig. 4a) and [2.2][5]helicenophane (±)-**3e** (Fig. 4b).[29] Viewed from the side, the facing triphenylenes and [5]helicenes strongly repel each other intramolecularly, forming curved structures with bulges in their center. Measuring the carbon–carbon distance between the two planes of [2.2]triphenylenophane (±)-**3a** revealed that although the shortest interplane distance (2.80 Å) is close to the value of [2.2]paracyclophane with the same diatomic bridge (2.83 Å), the longest interplane distance in the middle (3.68 Å) is considerably longer than that of [2.2]paracyclophane (3.09 Å). This central curvature is even more pronounced in [2.2][5]helicenophane (±)-**3e**, where the longest interplane distance is 4.08 Å. The top views of (±)-**3a** and (±)-**3e** show that the two oxamethylene tether chains are twisted rather than parallel as in [2.2]paracyclophane, with a larger twist angle in (±)-**3e** (136.5°) than in (±)-**3a** (55.1°). This large twist in (±)-**3e** may be due to the helical structure of the two [5]helicenes twisting and overlapping each other so that they do not repel each other. The helical chirality of the two [5]helicenes in **3e** was identical, and they were tethered together to form a long helicene-like structure. The dihedral angles of the two [5]helicenes were 51.9° and

© 2023 The Author(s). Published by the Royal Society of Chemistry

Open Access Article. Published on 10 March 2023. Downloaded on 2/5/2026 11:14:31 AM.
This article is licensed under a Creative Commons Attribution 3.0 Unported Licence.

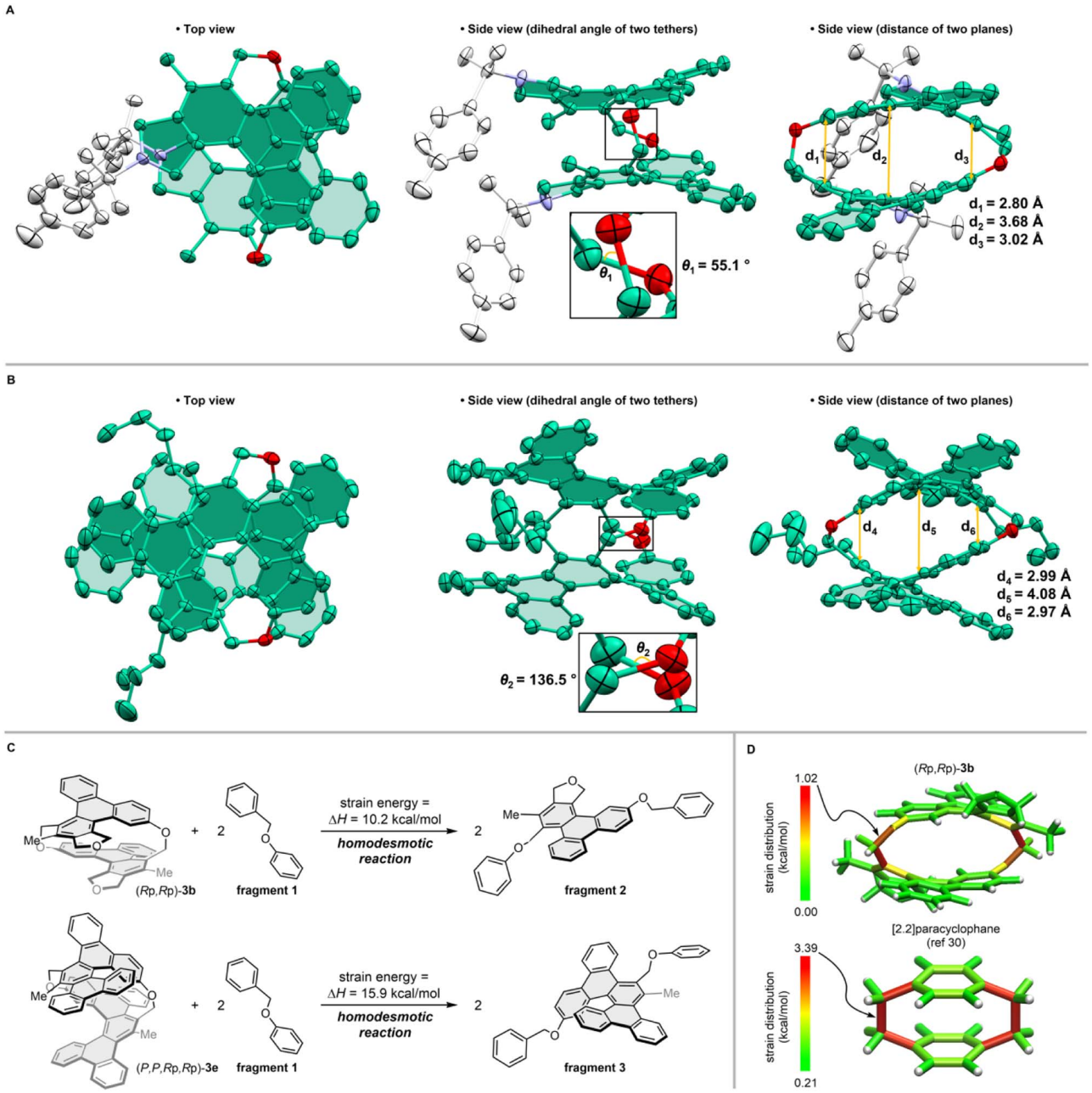

Fig. 4 X-ray crystal structures (a and b) and strain analyses (c and d). Hydrogen atoms are omitted for clarity. Atoms and the Ts group are colored green (carbon), red (oxygen), purple (nitrogen), and white (Ts group). (A) Unimolecular structures of [2.2]triphenylenophane (±)-**3a**. (B) Unimolecular structures of [2.2][5]helicenophane (±)-**3e**. (C) Strain energies of [2.2]triphenylenophane **3b** and [2.2][5]helicenophane **3e**. (D) StrainViz of **3b** and [2.2]paracyclophane.

55.0°, slightly smaller than the 56.2° of dibenzo[*f*,*j*]picene[30] (Fig. S5†).

We further evaluated the strain energies by DFT calculations at the B3LYP/6-31G(d) level. The strain energy calculated based on the homodesmotic reaction method[31] was greater for [2.2][5] heliceno-phane **3e** (15.9 kcal mol^{-1}) than for [2.2]triphenylenophane **3b** (10.2 kcal mol^{-1}) (Fig. 4c). The strain distribution analysis using StrainViz[32] showed that the strain of [2.2]triphenylenophane **3b** was unevenly distributed at the tethered moieties (Fig. 4d). These cyclophanes have smaller strain than [2.2]paracyclophane,[33] which may be due to strain dispersion by π-extension and increased flexibility of the tether by introducing oxygen atoms.

We examined the photophysical properties of [2.2]triphenylenophanes **3a–c** (Fig. 5a) and [2.2][5]helicenophane **3e** (Fig. 5b) and summarized the data in Table 2. The UV-vis absorption spectra of [2.2]triphenylenophanes **3a–c** showed absorption maxima at 267–269 nm, with little change due to substituent differences. On the other hand, the fluorescence spectra showed emission maxima at 406–450 nm, with a pronounced red shift

Open Access Article. Published on 10 March 2023. Downloaded on 2/5/2026 11:14:31 AM.
This article is licensed under a Creative Commons Attribution 3.0 Unported Licence.

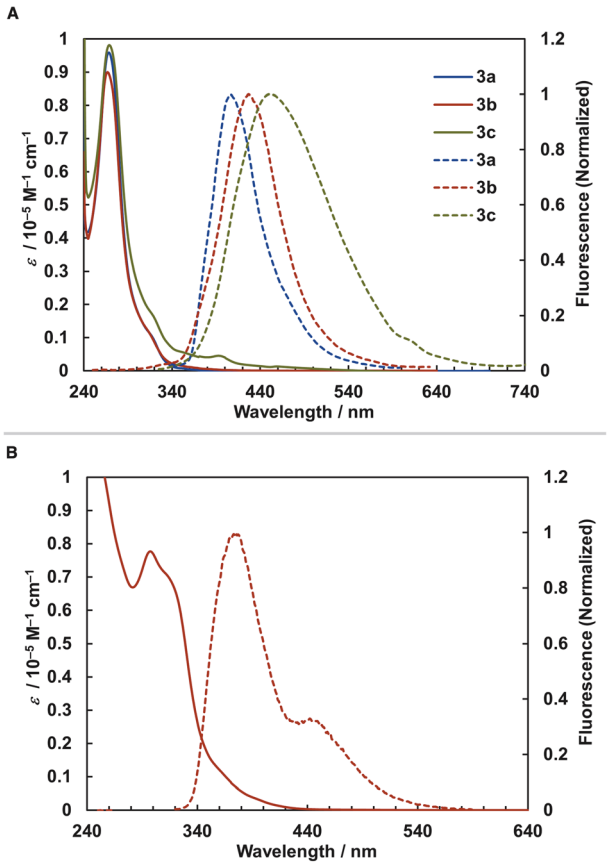

Fig. 5 Absorption (solid line) and emission (dashed line) spectra. (A) **3a**–**3c**. (B) **3e**

and broadening in the order of **3a**, **3b**, and **3c**. For [2.2][5]helicenophane **3e**, the absorption maximum was 297 nm on the longer wavelength compared to **3a–c**, resulting in a smaller Stokes shift. This phenomenon may be due to the higher molecular rigidity of helicene than triphenylene, which suppresses the structural relaxation of excited states.[34] Regarding fluorescence quantum yields, [2.2]triphenylenophanes **3a–c** showed very small values (0.6–2.1%) similar to that of [2.2]paracyclophanes without additional chromophores,[35] much smaller than that of unsubstituted triphenylene(9%).[36] In contrast, the fluorescence quantum yield of [2.2][5]helicenophane **3e** was 12.5%, a significant increase over the 4% of [5]helicene.[37]

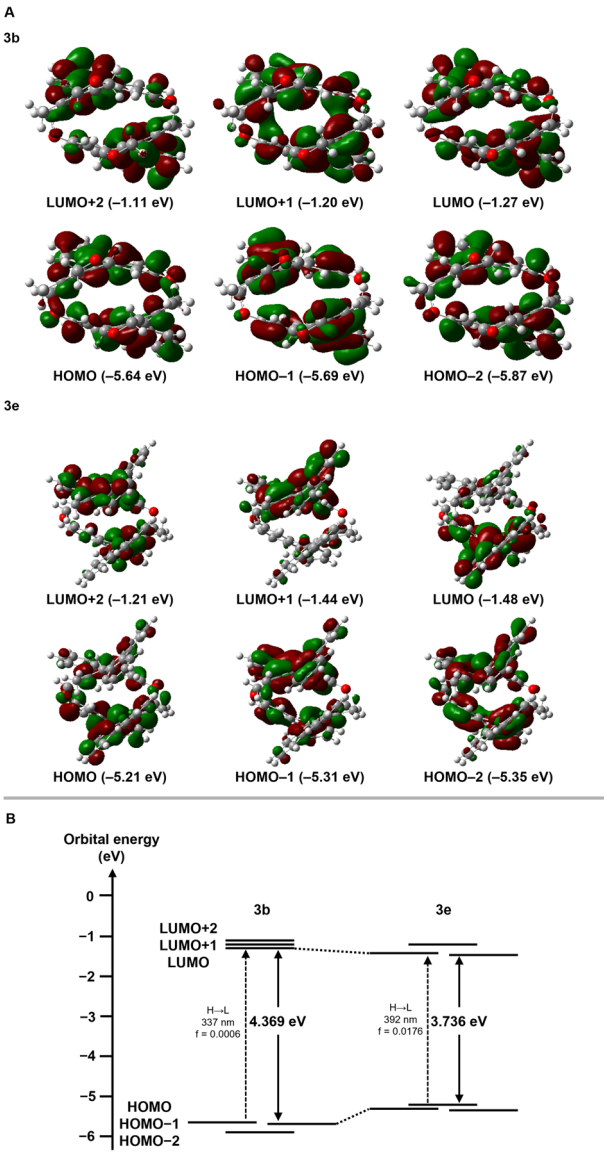

Fig. 6 Electronic structures calculated by TD-DFT at the B3LYP/6-31G(d) level. (A) Pictorial representations of six frontier MOs of **3b** and **3e**. (B) Energy diagrams of **3b** and **3e**.

To understand the optical properties described above, we examined the electronic properties of [2.2]triphenylenophane **3b** and [2.2][5]helicenophane **3e** by DFT and TD-DFT calculations at the B3LYP/6-31G(d) level. The frontier orbitals of **3b** and

Table 2 Photophysical and chiroptical data[a]

Compd	Absorption λ_{max}/nm	Emission λ_{max}/nm (excitation wavelength/nm)	Φ_F (excitation wavelength/nm)	$[\alpha]_D$[b] (ref. 25)	g_{abs}[c] (wavelength/nm)
(+)-**3a**	268	406 (310)	0.011 (290)	289	1.9×10^{-3} (325)
(+)-**3b**	267	427 (220)	0.021 (340)	255	1.6×10^{-3} (325)
(+)-**3c**	269	450 (305)	0.006 (300)	246	1.5×10^{-3} (331)
(+)-**3e**	297, 319	375, 446 (300)	0.125 (300)	940	3.9×10^{-3} (353)

[a] In CH_2Cl_2 (1.0×10^{-5} M) at 25 °C. [b] In $CHCl_3$ at 25 °C. [c] In $CHCl_3$ (1.0×10^{-5} M) at 25 °C.

© 2023 The Author(s). Published by the Royal Society of Chemistry

Open Access Article. Published on 10 March 2023. Downloaded on 2/5/2026 11:14:31 AM. This article is licensed under a Creative Commons Attribution 3.0 Unported Licence.

3e are delocalized and distributed throughout the molecule (Fig. 6a). For the transannular interactions between the two aromatic systems, an overlap of molecular orbitals was observed in the LUMO+1 orbital of **3b**. In contrast, no overlap was observed in any orbitals of **3e**. The energy diagrams of **3b** and **3e** are shown in Fig. 6b. The energy gap between the HOMO and LUMO orbitals is significantly narrower in **3e** (3.736 eV) than in **3b** (4.369 eV), supporting the experimental result that **3e** has absorption maxima at longer wavelengths than **3b**. The diagram reveals that decreasing the energy gap is mainly due to increasing occupied orbitals. This phenomenon may be due to the destabilization of the occupied orbitals of **3e**, which has a greater degree of curvature than **3b**. This structural dependence is also observed in cyclic π-conjugated compounds such as cycloparaphenylenes.[38] A comparison of the oscillator strength values of the interorbital transitions determined by TD-DFT calculations suggests that the HOMO → LUMO transition is almost forbidden for **3a** ($f = 0.0006$), whereas it is weak but permissible for **3e** ($f = 0.0176$).

Finally, we evaluated the chiroptical properties of [2.2]triphenylenophanes **3a–c**. The optical rotation values of **3a–c** and electronic circular dichroism (ECD) spectra of **3b** are shown in Table 2 and Fig. 7a, respectively. The optical rotation values of **3a–c** were 246–289°, larger than the planar chiral non-π-extended [2.2]paracyclophane.[39] The ECD spectra of **3b** show a mirror image based on the distinct Cotton effect, and the dissymmetry factor g_{abs} is moderate with a maximum value of 1.9×10^{-3}. This value is comparable to the planar chiral non-π-extended [2.2]paracyclophane.[3d,40] Enantiopure [2.2][5]helicenophanes (+)-**3e** and (−)-**3e** were also obtained by optical resolution of (±)-**3e** using chiral HPLC (Daicel CHIRALPAK IE). The optical rotation value of **3e** (940°) was significantly larger than those of **3a–c** and slightly larger than that of [2.2][4]helicenophane (878°) (Table 2).[8] The ECD spectra of (+)-**3e** and (−)-**3e** exhibited a mirror-image relationship (Fig. 7b). Similar to the optical rotation values, the dissymmetry factor g_{abs} (3.9×10^{-3}) was significantly larger than those of **3a–c**. The signs of the Cotton effects in the ECD spectra of (*Rp*,*Rp*)-**3b** and (*P*,*P*,*Rp*,*Rp*)-**3e** determined by the DFT calculations at the B3LYP/6-31G(d) level are in good agreement with the experimental spectra of (+)-**3b** and (+)-**3e**, and thus the absolute conformations of (+)-**3b** and (+)-**3e** was determined to be the *Rp*,*Rp* and *P*,*P*,*Rp*,*Rp* configurations, respectively.

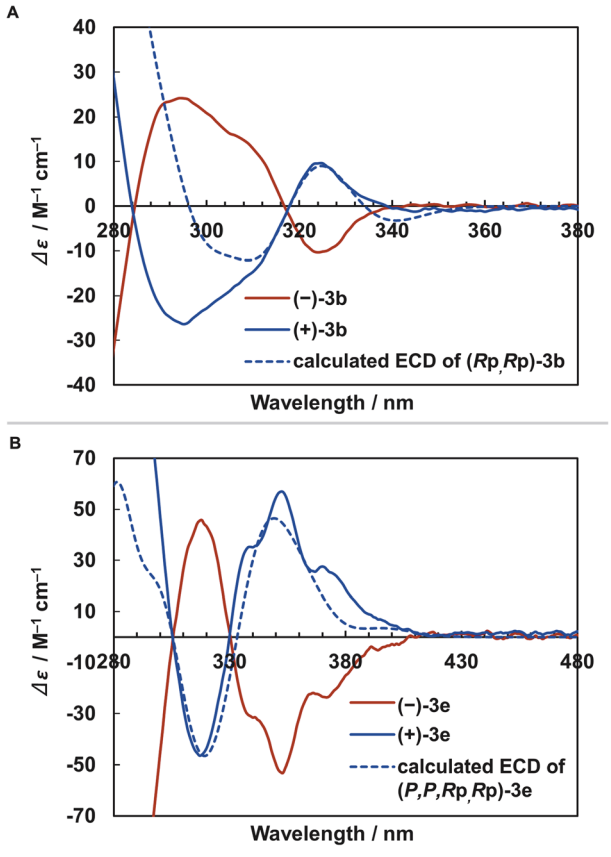

Fig. 7 ECD spectra. Dashed blue lines show ECD spectra calculated by TD-DFT at the B3LYP/6-31G(d) level. (A) (−)-**3b**, (+)-**3b**, and calculated (*Rp*,*Rp*)-**3b**. (B) (−)-**3e**, (+)-**3e**, and calculated (*P*,*P*,*Rp*,*Rp*)-**3e**.

Conclusions

In conclusion, we have succeeded in the diastereo- and enantioselective synthesis of the planar chiral [2.2] triphenylenophanes *via* the base-mediated intermolecular macrocyclization followed by the Rh-catalyzed asymmetric intramolecular double [2 + 2 + 2] cycloaddition. This asymmetric [2.2]cyclophane synthesis is the first example of diastereo- and enantioselective control of two planar chiralities of the [*n*.*n*]cyclophanes. We have also succeeded in the diastereoselective synthesis of planar chiral [2.2][5]helicenophane by the Ni-catalyzed intramolecular double [2 + 2 + 2] cycloaddition. The DFT calculations revealed that the diastereoselectivity of these reactions is kinetically determined by the second [2 + 2 + 2] cycloaddition rather than by rotational isomerization of the axial chirality of the biaryl intermediate produced in the first [2 + 2 + 2] cycloaddition. Single crystal X-ray diffraction analyses showed that the facing triphenylene skeletons strongly repel each other, leading to a curved structure with a bulged central part. Regarding photophysical properties, although fluorescence quantum yields of [2.2]triphenylenophanes (0.6–2.1%) are much smaller than that of unsubstituted triphenylene (9%), that of [2.2][5]helicenophane (12.5%) is much larger than that of [5]helicene (4%). Regarding the transannular interactions between the two aromatic rings, an overlap of molecular orbitals was observed in the [2.2]triphenylenophane, but no overlap was observed in the [2.2][5]helicenophane. Regarding chiroptical properties, the ECD spectra of the [2.2]triphenylenophane and the [2.2][5]helicenophane showed mirror images based on the distinct Cotton effects, and their dissymmetry factors g_{abs} are relatively good with maximum values of 1.9×10^{-3} for the [2.2]triphenylenophane and 3.9×10^{-3} for the [2.2][5]helicenophane. This study demonstrates that the transition-metal-catalyzed intramolecular double [2 + 2 + 2] cycloaddition is an excellent method for the stereoselective synthesis of PAHs-based [2.2] cyclophanes.

Open Access Article. Published on 10 March 2023. Downloaded on 2/5/2026 11:14:31 AM. This article is licensed under a Creative Commons Attribution 3.0 Unported Licence.

Data availability

Experimental procedures, spectral and crystal data, theoretical calculations, and characterization data for all new compounds are provided in the ESI.† Crystallographic data for compounds (±)-**3a** (CCDC 2237885) and (±)-**3e** (CCDC 2237886) have been deposited in the Cambridge Crystallographic Data Centre.

Author contributions

Y. K. designed the project and carried out experimental works. J. N. carried out X-ray crystal structure analyses and performed computational studies under the guidance of Y. N. Y. K. wrote a draft under the guidance of J. N. and Y. N. K. T. designed, advised, and directed the project and wrote the manuscript.

Conflicts of interest

There are no conflicts to declare.

Acknowledgements

This research was supported partly by Grants-in-Aid for Scientific Research (No. JP21K18949 and JP19H00893 to K. T., No. JP22H05346 to Y. N., and No. JP21J22287 to J. N.) from JSPS (Japan). We thank Dr Yoshio Ando and Prof. Ken Ohmori for their ^{1}H and ^{13}C NMR analyses of compound **2c** and Takasago International Corporation for the gift of segphos, H_8-binap, and xyl-H_8-binap. A generous allotment of computational resources from TSUBAME (Tokyo Institute of Technology) is gratefully acknowledged.

Notes and references

1 For reviews on cyclophanes, see: (*a*) I. Roy, A. H. G. David, P. J. Das, D. J. Pe and J. F. Stoddart, *Chem. Soc. Rev.*, 2022, **51**, 5557–5605; (*b*) R. López and C. Palomo, *Angew. Chem., Int. Ed.*, 2022, **61**, e202113504; (*c*) J.-R. Wu and Y.-W. Yang, *Chem. Commun.*, 2019, **55**, 1533–1543; (*d*) S. Kotha, M. E. Shirbhate and G. T. Waghule, *Beilstein J. Org. Chem.*, 2015, **11**, 1274–1331; (*e*) D. Ramaiah, P. P. Neelakandan, A. K. Nair and R. R. Avirah, *Chem. Soc. Rev.*, 2010, **39**, 4158–4168.

2 D. J. Cram, N. L. Allinger and H. Steinberg, *J. Am. Chem. Soc.*, 1954, **76**, 6132–6141.

3 For reviews on [2.2]paracyclophanes, see: (*a*) J.-M. Teng, D.-W. Zhang and C.-F. Chen, *ChemPhotoChem*, 2022, **6**, e202100228; (*b*) S. Felder, S. Wu, J. Brom, L. Micouin and E. Benedetti, *Chirality*, 2021, **33**, 506–527; (*c*) Z. Hassan, E. Spuling, D. M. Knoll and S. Bräse, *Angew. Chem., Int. Ed.*, 2020, **59**, 2156–2170; (*d*) Y. Morisaki and Y. Chujo, *Bull. Chem. Soc. Jpn.*, 2019, **92**, 265–274; (*e*) Z. Hassan, E. Spuling, D. M. Knoll, J. Lahann and S. Bräse, *Chem. Soc. Rev.*, 2018, **47**, 6947–6963.

4 (*a*) M. Watanabe, Y. Ono, T. Ishihara, Y. J. Chang and M. Shibahara, *Chem.–Eur. J.*, 2022, **28**, e202200790; (*b*) E. Elacqua and L. R. MacGillivray, *Eur. J. Org. Chem.*, 2010, **2010**, 6883–6894.

5 (*a*) C. J. Brown and A. C. Farthing, *Nature*, 1949, **164**, 915–916; (*b*) C. L. Coulter and K. N. Trueblood, *Acta Crystallogr.*, 1963, **16**, 667–676.

6 D. J. Cram and N. L. Allinger, *J. Am. Chem. Soc.*, 1955, **77**, 6289–6294.

7 For reviews on PAHs-based cyclophanes, see: (*a*) K. J. Weiland, A. Gallego and M. Mayor, *Eur. J. Org. Chem.*, 2019, **2019**, 3073–3085; (*b*) P. G. Ghasemabadi, T. Yao and G. J. Bodwell, *Chem. Soc. Rev.*, 2015, **44**, 6494–6518.

8 M. Tsuchiya, H. Maeda, R. Inoue and Y. Morisaki, *Chem. Commun.*, 2021, **57**, 9256–9259.

9 For other examples of stereoselective π-elongation cyclophane synthesis from [2.2]paracyclophanes, see: (*a*) S. Biswas, Z. A. Tabasi, L. N. Dawe, Y. Zhao and G. J. Bodwell, *Org. Lett.*, 2022, **24**, 5009–5013; (*b*) M. R. Rapp, W. Leis, F. Zinna, L. D. Bari, T. Arnold, B. Speiser, M. Seitz and H. F. Bettinger, *Chem.–Eur. J.*, 2022, **28**, e202104161; (*c*) S. Biswas, Z. A. Tabasi, J.-B. Lin, Y. Zhao and G. J. Bodwell, *Org. Lett.*, 2021, **23**, 5461–5465; (*d*) S. Biswas, C. S. Qiu, L. N. Dawe, Y. Zhao and G. J. Bodwell, *Angew. Chem., Int. Ed.*, 2019, **58**, 9166–9170; (*e*) H. F. Bettinger, R. Einholz, A. Göttler, M. Junge, M.-S. Sättele, A. Schnepf, C. S., S. Schundelmeier and B. Speiser, *Org. Chem. Front.*, 2017, **4**, 853–860; (*f*) R. Bula, M. Fingerle, A. Ruff, B. Speiser, C. Maichle-Mössmer and H. F. Bettinger, *Angew. Chem., Int. Ed.*, 2013, **52**, 11647–11650.

10 K. S. Unikela, Z. A. Tabasi, L. N. Dawe, Y. Zhao and G. J. Bodwell, *J. Org. Chem.*, 2021, **86**, 4405–4412.

11 Diastereoselective synthesis of a planar chiral [2.2]naphthalenophane has been reported *via* desulfurization. See: M. Haenel and H. A. Staab, *Tetrahedron Lett.*, 1970, **11**, 3585–3588.

12 For an example of a PAHs-based oxygen-containing [3.3.6]cyclophane, see: P. G. Ghasemabadi, Y. Zhao and G. J. Bodwell, *Eur. J. Org. Chem.*, 2021, **2021**, 3559–3568.

13 (*a*) K. Tanaka, T. Hori, T. Osaka, K. Noguchi and M. Hirano, *Org. Lett.*, 2007, **9**, 4881–4884; (*b*) K. Kanda, S. Oshima, T. Shizuno, R. Hamanaka, M. Fukai and T. Shibata, *Heterocycles*, 2014, **88**, 1355–1370.

14 Y. Morisaki, M. Gon, T. Sasamori, N. Tokitoh and Y. Chujo, *J. Am. Chem. Soc.*, 2014, **136**, 3350–3353.

15 For selected other examples of optical resolution of [*n.n*]cyclophanes, see: (*a*) F. Biliz and M. Cakici, *Eur. J. Org. Chem.*, 2021, **2021**, 4828–4834; (*b*) M. Shimada, Y. Yamanoi, T. Ohto, S.-T. Pham, R. Yamada, H. Tada, K. Omoto, S. Tashiro, M. Shionoya, M. Hattori, K. Jimura, S. Hayashi, H. Koike, M. Iwamura, K. Nozaki and H. Nishihara, *J. Am. Chem. Soc.*, 2017, **139**, 11214–11221; (*c*) Y. Morisaki, R. Sawada, M. Gon and Y. Chujo, *Chem.–Asian J.*, 2016, **11**, 2524–2527.

16 For recent reviews on [2 + 2 + 2] cycloadditions, see: (*a*) K. Cen, M. Usman, W. Shen, M. Liu, R. Yang and J. Cai, *Org. Biomol. Chem.*, 2022, **20**, 7391–7404; (*b*) P. Matton, S. Huvelle, M. Haddad, P. Phansavath and

© 2023 The Author(s). Published by the Royal Society of Chemistry

Open Access Article. Published on 10 March 2023. Downloaded on 2/5/2026 11:14:31 AM. This article is licensed under a Creative Commons Attribution 3.0 Unported Licence.

V. Ratovelomanana-Vidal, *Synthesis*, 2022, **54**, 4–32; (*c*) T. Gläsel, B. N. Baumann and M. Hapke, *Chem. Rec.*, 2021, **21**, 3727–3745.

17 For recent reviews on Rh-catalyzed [2 + 2 + 2] cycloadditions, see: (*a*) A. Pla-Quintana and A. Roglans, *Molecules*, 2022, **27**, 1332–1360; (*b*) Y. Shibata and K. Tanaka, Rhodium(I)-Catalyzed [2 + 2 + 2] and [4 + 2] Cycloadditions, in *Rhodium Catalysis in Organic Synthesis: Methods and Reactions*, ed. K. Tanaka, Wiley-VCH, Weinheim, 2019, pp. 183–228.

18 For a recent review on asymmetric [2 + 2 + 2] cycloadditions, see: A. Pla-Quintana and A. Roglans, *Asian J. Org. Chem.*, 2018, **7**, 1706–1718.

19 (*a*) Y. Aida, J. Nogami, H. Sugiyama, H. Uekusa and K. Tanaka, *Chem.–Eur. J.*, 2020, **26**, 12579–12588; (*b*) Y. Tahara, S. Obinata, K. S. Kanyiva, T. Shibata, A. Mándi, T. Taniguchi and K. Monde, *Eur. J. Org. Chem.*, 2016, **2016**, 1405–1413; (*c*) T. Araki, K. Noguchi and K. Tanaka, *Angew. Chem., Int. Ed.*, 2013, **52**, 5617–5621; (*d*) T. Shibata, M. Miyoshi, T. Uchiyama, K. Endo, N. Miura and K. Monde, *Tetrahedron*, 2012, **68**, 2679–2686; (*e*) T. Araki, D. Hojo, K. Noguchi and K. Tanaka, *Synlett*, 2011, **2011**, 539–542; (*f*) T. Shibata, T. Chiba, H. Hirashima, Y. Ueno and K. Endo, *Heteroat. Chem.*, 2011, **22**, 363–370; (*g*) T. Shibata, T. Uchiyama and K. Endo, *Org. Lett.*, 2009, **11**, 3906–3908; (*h*) K. Tanaka, H. Sagae, K. Toyoda, K. Noguchi and M. Hirano, *J. Am. Chem. Soc.*, 2007, **129**, 1522–1523.

20 For examples of enantioselective synthesis of chiral aromatic rings and belts by Rh-catalyzed intramolecular [2 + 2 + 2] cycloadditions, see: (*a*) J. Nogami, Y. Nagashima, H. Sugiyama, K. Miyamoto, Y. Tanaka, H. Uekusa, A. Muranaka, M. Uchiyama and K. Tanaka, *Angew. Chem., Int. Ed.*, 2022, **61**, e202200800; (*b*) J. Nogami, Y. Nagashima, K. Miyamoto, A. Muranaka, M. Uchiyama and K. Tanaka, *Chem. Sci.*, 2021, **12**, 7858–7865; (*c*) J. Nogami, Y. Tanaka, H. Sugiyama, H. Uekusa, A. Muranaka, M. Uchiyama and K. Tanaka, *J. Am. Chem. Soc.*, 2020, **142**, 9834–9842; (*d*) S. Nishigaki, Y. Shibata, A. Nakajima, H. Okajima, Y. Masumoto, T. Osawa, A. Muranaka, H. Sugiyama, A. Horikawa, H. Uekusa, H. Koshino, M. Uchiyama, A. Sakamoto and K. Tanaka, *J. Am. Chem. Soc.*, 2019, **141**, 14955–14960.

21 For a review on cycloarylene synthesis *via* [2 + 2 + 2] cycloadditions, see: D. Kohrs, J. Volkmann and H. A. Wegner, *Chem. Commun.*, 2022, **58**, 7483–7494.

22 For examples of the cycloparaphenylene synthesis *via* Rh-catalyzed [2 + 2 + 2] cycloadditions, see: (*a*) D. Kohrs, J. Becker and H. A. Wegner, *Chem.–Eur. J.*, 2022, **28**, e202104239; (*b*) J. Volkmann, D. Kohrs, F. Bernt and H. A. Wegner, *Eur. J. Org. Chem.*, 2022, **2022**, e202101357; (*c*) L.-H. Wang, Y. Nagashima, M. Abekura, H. Uekusa, G. Konishi and K. Tanaka, *Chem.–Eur. J.*, 2022, **28**, e202200064; (*d*) N. Hayase, H. Sugiyama, H. Uekusa, Y. Shibata and K. Tanaka, *Org. Lett.*, 2019, **21**, 3895–3899; (*e*) N. Hayase, Y. Miyauchi, Y. Aida, H. Sugiyama, H. Uekusa, Y. Shibata and K. Tanaka, *Org. Lett.*, 2017, **19**, 2993–2996; (*f*) Y. Miyauchi, K. Johmoto, N. Yasuda, H. Uekusa, S. Fujii, M. Kiguchi, H. Ito, K. Itami and K. Tanaka, *Chem.–Eur. J.*, 2015, **21**, 18900–18904; (*g*) A.-F. Tran-Van, E. Huxol, J. M. Basler, M. Neuburger, J.-J. Adjizian, C. P. Ewels and H. A. Wegner, *Org. Lett.*, 2014, **16**, 1594–1597.

23 For examples of the triphenylene synthesis by [2 + 2 + 2] cycloadditions of diynes with monoynes, see: (*a*) J. D. W. Schepper, A. Orthaber and F. Pammer, *J. Org. Chem.*, 2021, **86**, 14767–14776; (*b*) K. Murayama, Y. Sawada, K. Noguchi and K. Tanaka, *J. Org. Chem.*, 2013, **78**, 6202–6210; (*c*) Y. Sawada, S. Furumi, A. Takai, M. Takeuchi, K. Noguchi and K. Tanaka, *J. Am. Chem. Soc.*, 2012, **134**, 4080–4083; (*d*) A. McIver, D. D. Young and A. Deiters, *Chem. Commun.*, 2008, 4750–4752; (*e*) D. Peña, S. Escudero, D. Pérez, E. Guitián and L. Castedo, *Angew. Chem., Int. Ed. Engl.*, 1998, **37**, 2659–2661, See also ref. 22c.

24 H. Shimizu, I. Nagasaki and T. Saito, *Tetrahedron*, 2005, **61**, 5405–5432.

25 For examples of the carbohelicene synthesis by Ni-catalyzed [2 + 2 + 2] cycloadditions, see: (*a*) M. Šámal, J. Rybáček, J. Holec, J. Hanus, J. Vacek, M. Buděšínský, L. Bednárová, P. Fiedler, M. Š. Slušná, I. G. Stará and I. Starý, *Chem. Commun.*, 2022, **58**, 12732–12735; (*b*) D. Sakamoto, I. G. Sánchez, J. Rybáček, J. Vacek, L. Bednárová, M. Pazderková, R. Pohl, I. Císařová, I. G. Stará and I. Starý, *ACS Catal.*, 2022, **12**, 10793–10800; (*c*) J. Klívar, M. Šámal, A. Jančařík, J. Vacek, L. Bednárová, M. Buděšínský, P. Fiedler, I. Starý and I. G. Stará, *Eur. J. Org. Chem.*, 2018, **2018**, 5164–5178; (*d*) J. Nejedlý, M. Šámal, J. Rybáček, M. Tobrmanová, F. Szydlo, C. Coudret, M. Neumeier, J. Vacek, J. V. Chocholoušová, M. Buděšínský, D. Šaman, L. Bednárová, L. Sieger, I. G. Stará and I. Starý, *Angew. Chem., Int. Ed.*, 2017, **56**, 5839–5843; (*e*) T. Tsujihara, N. Inaba-Nozaki, T. Takehara, D.-Y. Zhou, T. Suzuki and T. Kawano, *Eur. J. Org. Chem.*, 2016, **2016**, 4948–4952; (*f*) P. Aillard, P. Retailleau, A. Voituriez and A. Marinetti, *Chem. Commun.*, 2014, **50**, 2199–2201; (*g*) F. Teplý, I. G. Stará, I. Starý, A. Kollárovič, D. Šaman, L. Rulíšek and P. Fiedler, *J. Am. Chem. Soc.*, 2002, **124**, 9175–9180.

26 A. Jančařík, J. Rybáček, K. Cocq, J. V. Chocholoušová, J. Vacek, R. Pohl, L. Bednárová, P. Fiedler, I. Císařová, I. G. Stará and I. Starý, *Angew. Chem., Int. Ed.*, 2013, **52**, 9970–9975.

27 For reviews on mechanistic studies of the Rh-catalyzed [2 + 2 + 2] cycloaddition, see: (*a*) A. Roglans, A. Pla-Quintana and M. Solà, *Chem. Rev.*, 2021, **121**, 1894–1979; (*b*) L. Orian and F. M. Bickelhaupt, *Synlett*, 2021, **32**, 561–572.

28 For mechanistic studies on the rhodium-catalyzed [2 + 2 + 2] cycloaddition, see: (*a*) K. Fujii, Y. Nagashima, T. Shimokawa, J. Kanazawa, H. Sugiyama, K. Masutomi, H. Uekusa, M. Uchiyama and K. Tanaka, *Nat. Synth.*, 2022, **1**, 365–375; (*b*) D. Yokose, Y. Nagashima, S. Kinoshita, J. Nogami and K. Tanaka, *Angew. Chem., Int. Ed.*, 2022, **61**, e202202542; (*c*) Ò. Torres, M. Fernàndez, À. Díaz-Jiménez, A. Pla-Quintana, A. Roglans and M. Solà, *Organometallics*, 2019, **38**, 2853–2862; (*d*) A. Dachs, S. Osuna, A. Roglans and M. Solà, *Organometallics*, 2010, **29**, 562–569; (*e*) A. Dachs,

Open Access Article. Published on 10 March 2023. Downloaded on 2/5/2026 11:14:31 AM.
This article is licensed under a Creative Commons Attribution 3.0 Unported Licence.

A. Torrent, A. Pla-Quintana, A. Roglans and A. Jutand, *Organometallics*, 2009, **28**, 6036–6043; (*f*) L. Orian, J. N. P. van Stralen and F. M. Bickelhaupt, *Organometallics*, 2007, **26**, 3816–3830.

29 CCDC 2237885 [(±)-**3a**] and CCDC 2237886 [(±)-**3e**] contain the supplementary crystallographic data.

30 J. Seibel, O. Allemann, J. S. Siegel and K.-H. Ernst, *J. Am. Chem. Soc.*, 2013, **135**, 7434–7437.

31 Y. Segawa, A. Yagi, H. Ito and K. Itami, *Org. Lett.*, 2016, **18**, 1430–1433.

32 C. E. Colwell, T. W. Price, T. Stauch and R. Jasti, *Chem. Sci.*, 2020, **11**, 3923–3930.

33 S. M. Bachrach, *J. Phys. Chem. A*, 2011, **115**, 2396–2401.

34 H. Tanaka, Y. Inoue and T. Mori, *ChemPhotoChem*, 2018, **2**, 386–402.

35 J. W. Hong, H. Y. Woo, B. Liu and G. C. Bazan, *J. Am. Chem. Soc.*, 2005, **127**, 7435–7443.

36 C. A. Parker and T. A. Joyce, *Trans. Faraday Soc.*, 1966, **62**, 2785–2792.

37 J. B. Birks, D. J. S. Birch, E. Cordemans and E. V. Donckt, *Chem. Phys. Lett.*, 1976, **43**, 33–36.

38 T. Iwamoto, Y. Watanabe, Y. Sakamoto, T. Suzuki and S. Yamago, *J. Am. Chem. Soc.*, 2011, **133**, 8354–8361.

39 R. Sawada, M. Gon, J. Nakamura, Y. Morisaki and Y. Chujo, *Chirality*, 2018, **30**, 1109–1114.

40 Large circularly polarized luminescence dissymmetry factors (g_{lum}) are observed in propeller-shaped macrocyclic compounds with a [2.2]paracyclophane core. $g_{lum} = 8.4 \times 10^{-3}$, see: (*a*) M. Gon, H. Kozuka, Y. Morisaki and Y. Chujo, *Asian J. Org. Chem.*, 2016, **5**, 353–359; $g_{lum} = 1.0 \times 10^{-2}$, see: ; (*b*) M. Gon, Y. Morisaki and Y. Chujo, *J. Mater. Chem. C*, 2015, **3**, 521–529; $g_{lum} = 1.1 \times 10^{-2}$, see: ref. 14.

© 2023 The Author(s). Published by the Royal Society of Chemistry